Received: 27 August 2017 | Revised: 12 March 2018 | Accepted: 14 March 2018
DOI: 10.1002/fam.2524

RESEARCH ARTICLE

WILEY

A methodology for predicting and comparing the full-scale fire performance of similar materials based on small-scale testing*

Chad M. Lannon[1] | Stanislav I. Stoliarov[2] | James M. Lord[3] | Isaac T. Leventon[4]

[1] Holmes Fire LP, San Francisco 94104, USA

[2] University of Maryland, Department of Fire Protection Engineering, College Park 20742, USA

[3] Bureau of Alcohol, Tobacco, Firearms and Explosives, Fire Research Laboratory, Ammendale 20705, USA

[4] National Institute of Standards and Technology, Fire Research Division, Gaithersburg 20899, USA

Correspondence
Stanislav I. Stoliarov, University of Maryland, Department of Fire Protection Engineering, College Park 20742, USA.
Email: stolia@umd.edu

Summary

Reconstructive fire testing is an important tool used by fire investigators to determine the cause, origin, and progression of a particular fire. Accurate reconstruction of the fire requires the laboratory structure to be outfitted with materials that, in terms of contribution to fire growth, perform similarly to the original materials found at the fire scene. Therefore, a procedure was developed to enable fire investigators to select these replacement materials on the basis of a quantitative assessment of their relative fire performance. This procedure consists of gram-scale and/or milligram-scale standard testing accompanied by inverse numerical modeling of these tests, which is used to obtain relevant material properties. A numerical model composed of a detailed pyrolysis submodel and empirical flame heat feedback submodels, which were developed in this study, is subsequently employed to simulate the early stages of the Room Corner Test, which was selected to represent full-scale material performance. The results of these simulations demonstrate that this procedure can successfully differentiate between fire growth propensities of several commercially available medium density fiberboards.

KEYWORDS

flame spread, forensic fire reconstruction, MDF, pyrolysis, Room Corner Test, ThermaKin

1 | INTRODUCTION

An effective method in determining the cause, origin, and progression of a fire is to perform reconstructive fire tests. A reconstructive fire test strives to recreate a fire that is under investigation by building a full-scale replica of the structure in a laboratory and using it to test hypotheses. When building these structures, it is often necessary to substitute materials that are commercially available for the original materials that were found during the fire investigation because the original materials were either destroyed or there is an insufficient quantity remaining to conduct large scale tests. NFPA 921: Guide for Fire and Explosion Investigations states that the reconstructive fire test is only credible when the materials utilized in the test assembly are "suitable exemplars of the actual materials".[1] Accurate reconstructive fire testing requires these materials to behave similarly to the original materials during the likely fire scenario.

Currently, materials are chosen for use in reconstruction tests based on the information available about the construction of the building and/or through post-fire visual examination of the remaining materials. The fire forensic field needs a quantitative methodology for comparing various materials and predicting how they perform relative to one another in a full-scale fire scenario so that substitute materials can be better selected for reconstructive fire testing. The goal of this study is to develop a systematic procedure that allows fire investigators to obtain relevant properties of several similar materials and then compare their fire performance through modeling of a full-scale fire scenario. The selected full-scale scenario was the NFPA

*This work was carried out by the National Institute of Standards and Technology (NIST), an agency of the US government and by statue is not subject to copyright in USA. The identification of any commercial product or trade name does not imply endorsement or recommendation by NIST. The policy of NIST is to use metric units of measurement in all its publications, and to provide statements of uncertainty for all original measurements. In this document, however, data from organizations outside NIST are shown, which may include measurements in non-metric units or measurements without uncertainty statements.

Copyright © 2018 John Wiley & Sons, Ltd.

286 Room Corner Test.[2] This scenario was selected because it is routinely used to evaluate fire performance of internal wall lining materials, which tend to be major contributors to fires in residential structures.

2 | BACKGROUND

The Room Corner Test is a standard test used to evaluate the flammability of combustible wall and ceiling materials and measure their potential overall contribution to fire growth during a compartment fire. In this test, a compartment is constructed, the interior walls and/or ceiling are lined with the test sample, and a gas burner is placed on the floor in the corner of the room. Once the gas burner fire ignites the combustible wall material, flames usually spread upward at a significant rate due to corner-wall re-radiation and reduced air entrainment rate.[3] If the wall and/or ceiling material is sufficiently flammable, the fire will continue to spread along the corner-walls and ceiling until the compartment transitions to flashover, provided that sufficient fuel is available.

During the Room Corner Test, early fire growth is primarily dictated by the rate of upward flame spread along the corner walls. Upward flame spread was described by Saito et al[4] as a process that involves 3 zones along the vertical combustible surface: pyrolysis, flame extension, and burnout. In the pyrolysis zone, flames continuously exist over the combustible surface because the material has ignited and gaseous fuel is being produced. The material has not ignited in the flame extension zone but is being preheated by the fluctuating flame and radiation from surrounding surfaces and ceiling smoke layer. In the burnout zone, flames do not exist because the material is no longer producing sufficient amount of fuel to sustain combustion.

Significant efforts have been made to study flame height and heat flux along the corner-wall and ceiling due to an exposure fire or a wall material fire.[5-13] Experiments were performed in either a compartment similar to the Room Corner Test or in an open corner-wall assembly. Lattimer and Sorathia[13] performed detailed experiments characterizing the steady-state heat flux and gas temperature at the surface of the walls and ceiling during a fire in the corner of a room. They used a square propane burner to represent an exposure fire and a thin propane line burner to represent the burning surface of 2 corner walls. Correlations for the flame height, gas temperature, and heat flux to the walls and ceiling were developed to represent both scenarios. These correlations state that the heat flux in the lower half of a corner-wall flame is 70 kW m^{-2}, and the peak heat flux from the squarer gas burner is 59, 84, and 104 kW m^{-2} when the square gas burner is 0.17, 0.3, and 0.5 m wide, respectively.

Lattimer and Sorathia[14] also performed flame spread experiments where combustible materials lined the walls and ceiling in the open corner-wall configuration and were exposed to the ISO 9705 burner conditions. Overall, their flame height correlation[13] predicted the experimental measurements well; however, during the early stages of burner exposure and flame spread, model predictions of heat flux were notably greater than experimental measurements. It is important to note that that the majority of the corner-wall fire studies focused on the heat feedback from a square gas burner that replicated the burner output in a standard test or a gaseous line burner that was intended to mimic a corner-wall material fire. Few researchers measured the thermal conditions of a fire spreading on an actual combustible wall lining.

Driven by the importance of this scenario and the high cost of the Room Corner Test, a number of models of variable complexity have been developed to simulate its dynamics. Quintiere[15] developed one of the first room corner fire models, and his overall approach was later adopted by many other researchers.[16-20] Quintiere's model relied on the upward flame spread model developed by Saito et al[4] and a simple upper layer gas temperature correlation to determine radiative heat transfer from the smoke. Flame spread occurred once the surface temperature reached the prescribed ignition temperature. The pyrolysis zone then produced heat and the total heat release rate (HRR) was tracked in time for the entire compartment. Flashover was assumed to occur at HRR = 1.0 MW. Heat flux to the wall was specified to be 60 and 30 kW m^{-2} in the pyrolysis zone and flame extension zones, respectively. Several bench-scale tests including cone calorimetry[21] and the Lateral Ignition and Flame Spread test[22] were performed to obtain the material properties, which served as inputs to the model. Dillon[12] demonstrated that Quintiere's model was sensitive to the material properties obtained through bench-scale testing, and the model's predictions could be fit to the Room Corner Test results once the heat of gasification and total combustion energy produced per unit area of material were increased or decreased.

The Building Research Association of New Zealand (BRANZ) developed the B-RISK model[23] that is considered to be the state-of-the-art and is among few publicly available compartment fire models designed to simulate the Room Corner Test. The corner-wall fire growth model within B-RISK relies on Lattimer's flame height and peak burner heat flux correlations[13] from an exposure fire to characterize the thermal conditions along the surface of a corner-wall material. The fire growth model is coupled to a zone model. More specifically, the fire growth model uses the upper layer temperature predicted by the zone model to determine the additional heat flux to the material surfaces. During validation,[23] B-RISK was shown to adequately predict the overall compartment HRR curves. However, it notably over-predicted early HRR, when the impact of the properties of the wall lining material is arguably most pronounced.

3 | GENERAL APPROACH

A 2-dimensional burning model, ThermaKin2D, was selected to simulate the critical aspect of the Room Corner Test—upward flame spread along the corner walls. The 2 dimensions resolved in the model corresponded to the height and thickness of these walls. The governing equations of ThermaKin2D, together with a description of the solution methodology and verification exercises, can be found in an earlier publication.[24] Unlike modeling tools previously utilized for the simulation of this test, ThermaKin2D is based on a highly detailed representation of physical and chemical processes involved in condensed-phase pyrolysis. As a consequence, this model requires an extensive set of material properties. In this work, these properties were obtained through inverse modeling of standard bench-scale and/or milligram-scale material tests. ThermaKin2D was used to carry out the inverse modeling of these tests.

Simulation of flame spread along the corner walls required development of empirical flame submodels to represent heat feedback to the material surface from an ignition source (square gas burner) and from a spreading corner-wall flame supported by the combustible wall lining material. Therefore, tests were conducted in an open corner-wall assembly to characterize heat feedback from these sources. The complete flame spread model, containing pyrolysis and flame submodels, was employed to model a series of Room Corner Tests performed on similar materials. The model's ability to predict differences in the test outcomes was evaluated.

4 | MATERIAL PROPERTY DETERMINATION PROCEDURE

4.1 | Materials

Medium density fiberboard (MDF), an engineered wood product, was selected as the target material because it is widely used in both modern and legacy construction. Four types of internal wall paneling were acquired from building supply stores; each type was identified as MDF. The materials were produced by 3 different manufacturers in varying thickness (τ), density (ρ), and finish colors and textures (either smooth or with a "bead", a groove incorporated into the MDF for esthetic purposes). Gypsum wallboard was also used in this study as backing material onto which the MDF was mounted in accordance with the NFPA 286.[2] A summary of the information on all these materials is provided in Table 1. Prior to testing, the MDF samples and gypsum wallboard were conditioned at 296 K and 50% humidity until the sample mass reached equilibrium.

4.2 | Procedure

The authors of this study have previously developed a systematic procedure for parametrization of pyrolysis models for combustible solids.[25] In this procedure, key physical and chemical processes and properties are isolated and systematically determined through a combination of experiments and modeling. Unfortunately, this procedure relies on a set of instruments including the Controlled Atmosphere Pyrolysis Apparatus and differential scanning calorimetry that are not readily available to the fire investigation community. Therefore, a decision was made not to use this procedure in this study and to create a new procedure that relies only on standard, widely used flammability test methods: microscale combustion calorimetry (MCC) and cone calorimetry (CC).

MCC experiments were conducted in accordance with ASTM D7309[26] using 2 to 3-mg material samples that were pyrolyzed in nitrogen at a heating rate of 1 K s^{-1}. The HRR normalized by the initial mass (HRR/m_0) was collected as a function of the sample temperature. The heat of complete combustion of gaseous pyrolyzates (ΔH_c) and solid residue or char yield (θ_C) were determined. Each material was sampled and tested 5 times to ensure reproducibility.

CC experiments were performed in accordance with ASTM E1354.[21] Multiple tests were conducted at a range of incident radiant heat fluxes (q''_{inc}) between 20 and 80 kW m^{-2} on each material, and each test was repeated 3 times. MDF samples were stapled to the gypsum wallboard to replicate the installation practice used in the full-scale tests conducted in this study. Because MDF samples had a tendency to swell and delaminate during experiments, an edge frame[21] was employed to provide additional sample shape control. The HRR per unit area (HRRPUA) was measured as a function of time, and the effective heat of combustion of the gaseous pyrolyzates (ΔH_{eff}) was determined as the integral of HRRPUA from the time of ignition until the moment when flaming combustion became unstable and transitioned to smoldering divided by the corresponding area-normalized sample mass loss.

Two approaches to the material property evaluation were exercised. In the first approach, it was assumed that the fire investigator was only able to collect enough material for MCC testing (less than 50 mg is required). Modeling was used to fit the HRR/m_0 curves to determine the kinetics of the thermal decomposition reactions including the pre-exponential factors (A), activation energies (E), and stoichiometric yields (θ) of condensed-phase products. The measured heat of complete combustion, ΔH_c, was assigned to the gaseous pyrolyzates. The rest of the required material properties, including the heats of decomposition reactions (h) and component heat capacities (c), thermal conductivities (k), radiation absorption coefficients (α), and surface emissivities (ε) were assumed to have characteristic values computed as the averages of results measured for a wide range organic polymeric solids.[27]

In the second approach, the fire investigator was assumed to collect enough material to conduct both MCC and CC tests at multiple q''_{inc}. Similar to the first approach, MCC data were used to evaluate the kinetics of material decomposition; however, CC experiments provided the effective heat of combustion, ΔH_{eff}, and char density. Finally, the CC HRRPUA data were fit, using a model of this experiment implemented within ThermaKin2D, by manually changing remaining chemical, thermal, and optical properties until the model predictions matched the experimental results. The manual optimization was aided

TABLE 1 Materials used in this study

Name	Manufacturer	Description	τ, mm	ρ, kg m^{-3}
Sample A	Georgia-Pacific	White finish with a bead	6.2	1090
Sample B	Decorative Panels International	White finish with a bead	4.1	890
Sample C	Georgia-Pacific	Light brown finish with a bead	3.6	890
Sample D	Eucatex North America	Dark brown finish, smooth	3.2	1080
Gypsum wallboard	United States Gypsum	Paper-face sheathing	12.6	480

by an analysis of literature measurements, which was used to establish plausible limits for each property value. It should be noted that, as has been observed by other researchers,[28] the properties determined through this type of optimization procedure tend to be interdependent and, therefore, are expected to provide reasonable predictions only when used as a complete set and only within the range of experimental conditions from which they were derived.

5 | MATERIAL PROPERTY DETERMINATION RESULTS

5.1 | MCC tests

The mean experimental MCC HRR/m_0 curves obtained for the MDF materials are shown in Figure 1 as points. A summary of these results is provided in Table 2. All uncertainties were computed from the scatter of the experimental data as 2 standard deviations of the mean.

ThermaKin2D simulations of the MCC tests were performed in a thermally thin (zero-dimensional) mode, where the temperature of the solid was forced to follow the set heating rate (1 K s^{-1}), and mass transport was effectively infinitely fast, in order to determine the decomposition kinetics from the MCC data. The decomposition reaction mechanism was assumed to consist of either a single reaction (1 Reaction Model):

$$\textit{Virgin Material} \rightarrow \theta_C\ \textit{Char} + (1-\theta_C)\ \textit{Gas} \tag{1}$$

or 2 consecutive reactions (2 Reaction Model):

$$\textit{Virgin Material} \rightarrow \theta_I\ \textit{Intermediate} + (1-\theta_I)\ \textit{Gas}_1 \tag{2}$$

TABLE 2 Summary of MCC test results

Sample	ΔH_c, J kg^{-1}	θ_C, %
A	(12.8 ± 1.2) × 10^6	17.5 ± 3.1
B	(13.9 ± 0.8) × 10^6	14.4 ± 6.3
C	(12.6 ± 1.2) × 10^6	17.6 ± 0.4
D	(14.1 ± 0.7) × 10^6	11.6 ± 2.4

$$\textit{Intermediate} \rightarrow \theta_{CI}\ \textit{Char} + (1-\theta_{CI})\ \textit{Gas}_2$$

All reactions were assumed to be first order. All gaseous products were assumed to have the heats of complete combustion, ΔH_c, listed in Table 2. The reaction parameters were determined using a manual fitting of the HRR/m_0 curves following the same approach that was previously employed for the fitting of thermogravimetric analysis data.[29,30] Acceptance criteria for this optimization procedure required model-predicted peak HRR/m_0, the temperature at which this peak occurs, and total heat release to match experimental measurements within 2.5%, 2.5%, and 0.5%, respectively.

The results of these fitting exercises are shown in Figure 1 as lines. The resulting kinetic parameters are given in Table 3. The 1 Reaction Model captures experimental data with coefficients of determination R^2 = 0.91–0.93. The 2 Reaction Model provides a notably better fit with R^2 = 0.96–0.99. In addition to these mechanisms, a decomposition mechanism consisting of 3 parallel reactions that was proposed by Li et al[31] for MDF was considered. The kinetic parameters of individual reactions determined by these researchers were kept unaltered, while the relative amounts of 3 reactants, which according to Li et al represent cellulose, hemicellulose, and adhesive, were varied to fit the MCC data. This exercise did not yield high quality fits for all

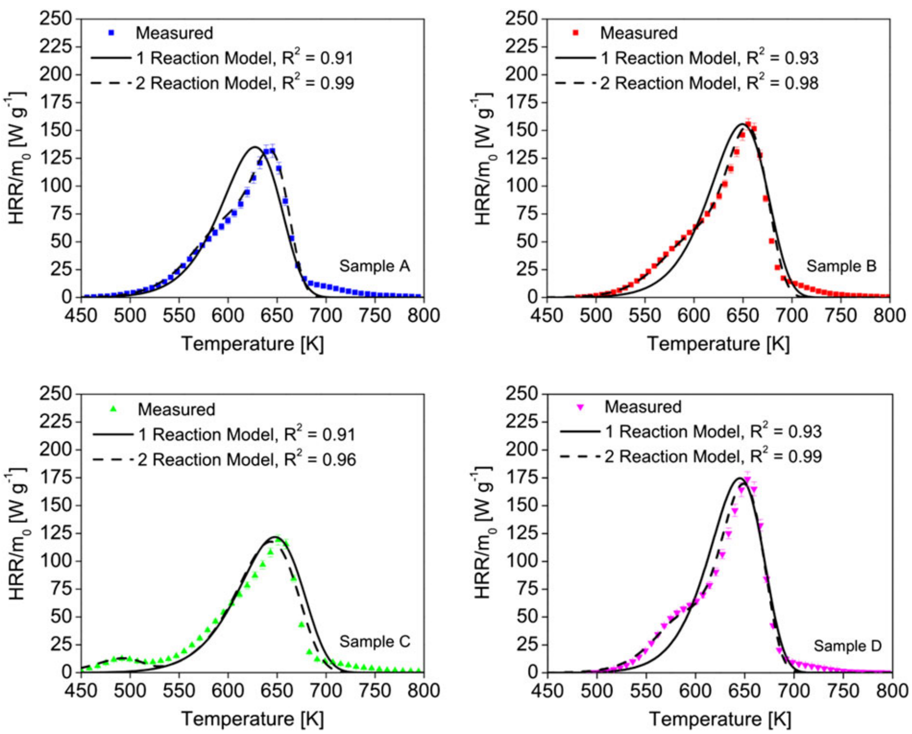

FIGURE 1 Experimentally measured and model predicted MCC heat release rates obtained for MDF samples at a heating rate of 1 K s^{-1} [Colour figure can be viewed at wileyonlinelibrary.com]

TABLE 3 MDF thermal decomposition kinetics derived from MCC experiments

Property	Sample A	Sample B	Sample C	Sample D
1 Reaction Model				
θ_C [%]	17.5	14.4	17.6	11.6
A [s^{-1}]	1.44×10^7	5.81×10^7	4.80×10^6	2.80×10^8
E [J mol^{-1}]	1.04×10^5	1.15×10^5	1.019×10^5	1.223×10^5
2 Reaction Model				
θ_I [%]	70.6	80.0	94.0	83.0
A_I [s^{-1}]	2.60×10^7	9.50×10^7	3.00×10^7	9.90×10^8
E_I [J mol^{-1}]	9.99×10^4	1.06×10^5	8.34×10^4	1.15×10^5
θ_{CI} [%]	24.8	18.0	18.8	13.9
A_{CI} [s^{-1}]	1.80×10^{11}	1.40×10^{10}	9.90×10^6	1.95×10^{10}
E_{CI} [J mol^{-1}]	1.55×10^5	1.45×10^5	1.05×10^5	1.45×10^5

materials (R^2 = 0.70–0.94), and, therefore, this approach was abandoned in favor of the simpler mechanisms.

5.2 | CC tests

The results of CC experiments performed on MDF samples are shown in Figures 2 to 4. The data in these figures are grouped in accordance with the imposed heat flux, q''_{inc}. The experimental data are shown as shaded areas, which indicate scatter between repeated tests. After several repeated CC experiments, the char mass was measured, and its structure was geometrically analyzed to determine the effective char density. Samples C and D produced char that maintained a solid structure, which made this determination relatively straightforward. The char produced by Samples A and B lacked structural integrity. Based on the observation that the overall sample thickness changed minimally during the tests on these materials, the volume of the char was estimated to be equal to the volume of the virgin sample. The effective heats of combustion, ΔH_{eff}, and char densities derived from CC experiments are summarized in Table 4.

Several additional CC experiments were conducted on Samples A and B, in which a water-cooled Schmidt-Boelter heat flux gauge was inserted into an orifice drilled through the sample and gypsum wallboard. The gauge surface was positioned flush with the top sample surface either at the center or near an edge of the sample. These experiments were used to estimate the contribution of the surface flame to the heat flux incident onto the samples, which is needed to accurately define thermal boundary conditions in the model of the CC experiments. Details of these heat flux measurements can be found elsewhere.[32] The mean flame heat flux over the exposed surface area of the sample was found to be 20 kW m^{-2}. Similar values were obtained in earlier studies for non-charring polymers burning in a comparable configuration.[33,34]

Cone calorimeter experiments were simulated in ThermaKin2D in a 1-dimensional mode. These simulations were repeated for each MDF sample using both the 1 Reaction and 2 Reaction Models for thermal decomposition. Convective cooling of the top sample surface prior to ignition was defined by the convection coefficient of 10 W m^{-2} K^{-1} and an environmental temperature of 300 K[35]. The additional heat flux from the flame (20 kW m^{-2}) was assumed to be radiative in nature[33] and added to q''_{inc} after ignition. Ignition was modeled to occur when the top surface mass flux of gaseous pyrolyzates reached a critical value, $\dot{m}''_{crit}$. The transport of the gases

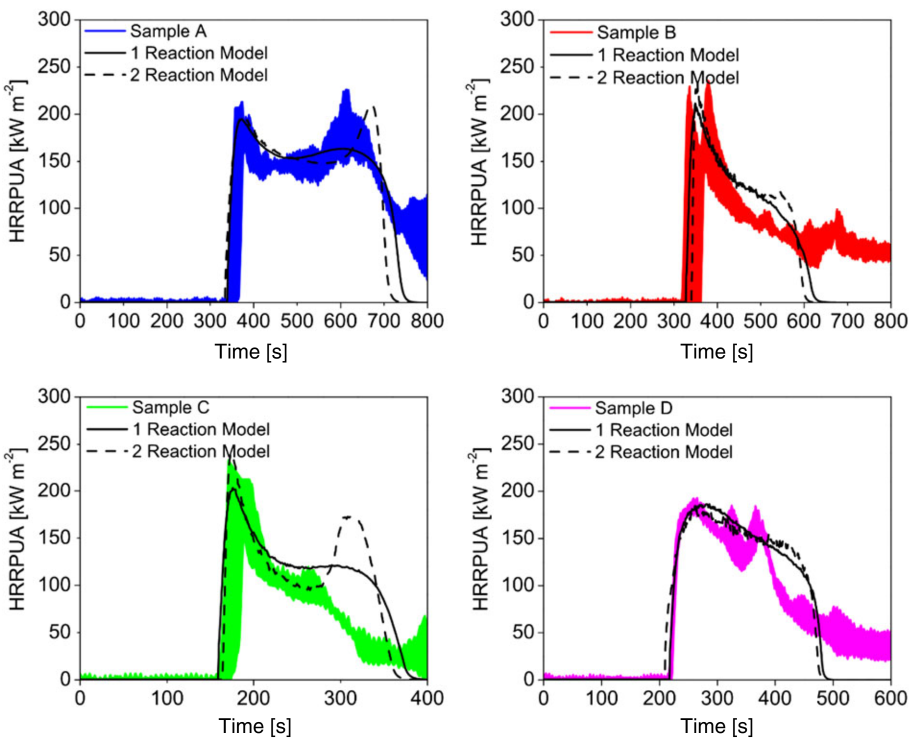

FIGURE 2 Experimentally measured (shaded area) and model predicted CC heat release rates for MDF samples exposed to q''_{inc}=20 or 25 kW m^{-2}. Sample C was the only material tested at 25 kW m^{-2} because it did not ignite at the lower heat flux [Colour figure can be viewed at wileyonlinelibrary.com]

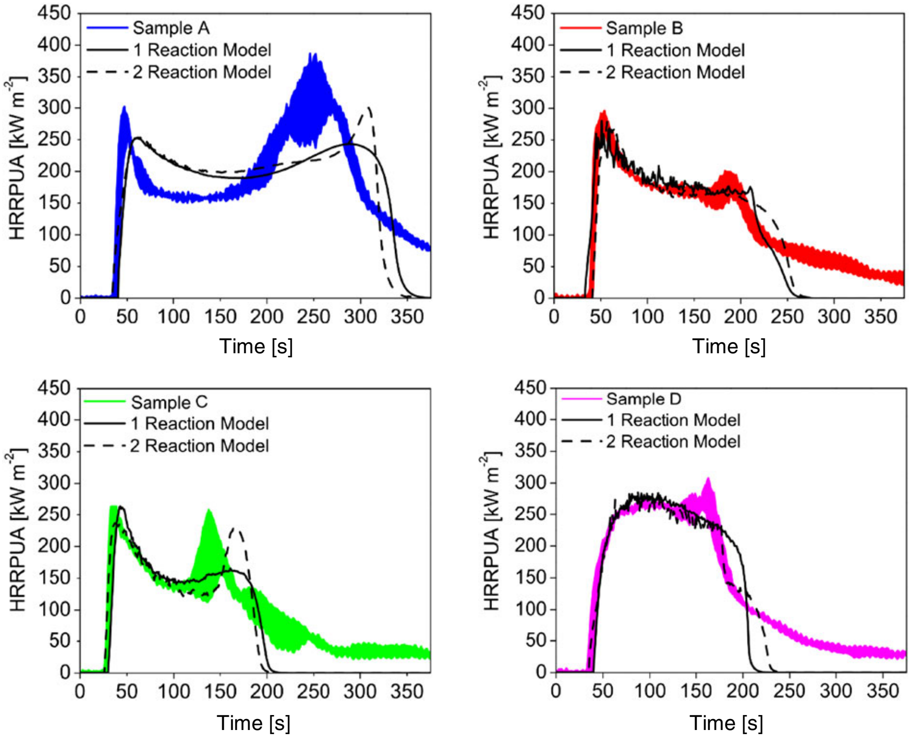

FIGURE 3 Experimentally measured (shaded area) and model predicted CC heat release rates for MDF samples exposed to q''_{inc}=50 kW m^{-2} [Colour figure can be viewed at wileyonlinelibrary.com]

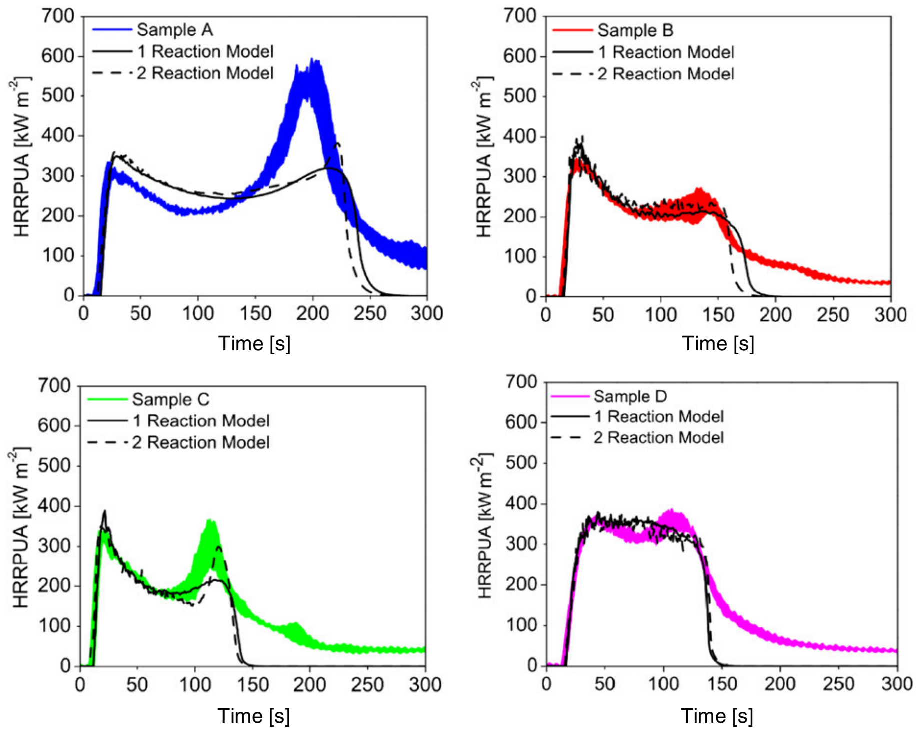

FIGURE 4 Experimentally measured (shaded area) and model predicted CC heat release rates for MDF samples exposed to q''_{inc}=80 kW m^{-2} [Colour figure can be viewed at wileyonlinelibrary.com]

through the solid to the top surface was specified to occur at a rate that would not inhibit their flow (ie, without resistance). The presence of gypsum wallboard behind the MDF samples was modeled explicitly using the properties obtained from the literature.[36] A brief study was conducted to ensure that the numerical integration parameters employed in these simulations provide fully converged results.[32]

The heat of combustion of all gaseous pyrolyzates was set equal to the corresponding ΔH_{eff}. The heat capacity of gaseous pyrolyzates

TABLE 4 Summary of CC test results

Sample	ΔH_{eff}, J kg^{-1}	Char Density, kg m^{-3}
A	$(11.3 \pm 8.6) \times 10^6$	191
B	$(11.7 \pm 10.8) \times 10^6$	128
C	$(10.3 \pm 11.7) \times 10^6$	382
D	$(12.9 \pm 5.9) \times 10^6$	255

was set to 1800 J kg^{-1} K^{-1}.[37] The heats of reactions and the thermal transport properties of the virgin sample, intermediate, and char (including k, c, ε, and α) were varied to fit the experimental CC data. A literature review on pyrolysis properties of synthetic polymers[27,38] and lignocellulosic materials[32,39-41] was conducted to define the average, minimum, and maximum values of each of these properties; these values are summarized in Table 5. The thermal conductivity of char was expressed as a function of temperature, T in Kelvin, using the radiation diffusion approximation to reflect the fact that heat flow through the char's porous structure is frequently dominated by radiation.[40] The emissivity and heat capacity of char were not varied and instead were set to typical values, 0.86 and 1500 J kg^{-1} K^{-1},[38] respectively. One additional parameter that was varied was $\dot{m}''_{crit}$. The variation of this parameter was constrained by the limits suggested by Lyon and Quintiere[42]:

$$15 \ \text{kW m}^{-2} \leq \left(\dot{m}''_{crit} * \Delta H_{eff}\right) \leq 27 \ \text{kW m}^{-2}$$

The properties listed in Table 5 and $\dot{m}''_{crit}$ were varied within their limits, in a manually iterative process, to produce the best agreement between model-predicted and experimentally measured ignition time and HRRPUA profiles. This procedure was informed by a previously conducted sensitivity analysis[27] that identified which properties exert the greatest influence on particular aspects of HRRPUA curves. Acceptance criteria for this optimization required model-predicted ignition time, first peak HRRPUA, and instantaneous HRRPUA obtained for the first 50% of quasi-steady burning period to match experimental measurements within 5 s, 10%, and 15%, respectively. For samples exposed to an incident heat flux of 20 or 25 kW m^{-2}, the optimization target for ignition time was relaxed to ±10 s, which is consistent with measured variations between repeated experiments. Additionally, when Sample A was exposed to an incident heat flux of 50 kW m^{-2}, 2 peaks in HRRPUA were measured, each approximately 100% higher than the average HRRPUA during the quasi-steady burning; thus, for this material, at this heat flux, the third optimization target was relaxed from 15% to 20%. Details of this optimization process can be found elsewhere.[32]

The results of these fitting exercises are shown in Figures 2 to 4 as lines. The best agreement between the model and experiments was achieved for Samples B and D. Throughout the full duration of quasi-steady burning, the average relative difference between experimentally measured and model-predicted HRRPUA for these materials was less than 12%. Although simulations using the 2 Reaction Model better capture the presence of second HRRPUA maxima observed in some experiments, the relative difference between experimentally measured and model-predicted HRRPUA data was found to be essentially the same for both reaction schemes. Consequently, the 1 Reaction Model was chosen for all simulations of full-scale experiments as it provided comparable accuracy, while requiring fewer parameters. Table 6 lists optimized property sets corresponding to this model. Material properties required for the 2 Reaction Model are listed in Table SI-1 of the Supplementary Information document.

6 | FLAME SUBMODEL DEVELOPMENT

6.1 | Open corner-wall experiments

An open corner-wall assembly, consisting of two 2.4-m tall, 1.2-m wide perpendicular walls with a partial ceiling was constructed under the 1-MW rated exhaust hood at the Bureau of Alcohol, Tobacco, Firearms and Explosives, Fire Research Laboratory (ATF FRL) as shown in Figure 5. This assembly was used to conduct 2 types of experiments: burner exposure and flame spread tests. Burner

TABLE 5 Pyrolysis property ranges for polymeric solids. Negative h indicates endothermic reactions

Property	Average	Minimum	Maximum
Virgin material and intermediate			
k [W m^{-1} K^{-1}]	0.24[a]	0.07[b]	0.42[a]
c [J kg^{-1} K^{-1}]	2300[a]	1100[c]	2900[a]
ε [−]	0.88[a]	0.70[d]	0.94[a]
α [m^2 kg^{-1}]	3.0[a]	0.6[a]	100[e]
h [J kg^{-1}]	-7×10^5[a]	-2.5×10^6[a]	0[f]
Char			
k [W m^{-1} K^{-1}]	$5 \times 10^{-10} \times T^3$[d]	$1 \times 10^{-10} \times T^3$[d]	$1 \times 10^{-9} \times T^3$[d]
α [m^2 kg^{-1}]	10[a]	0.6[a]	100[e]

[a]Stoliarov et al.[27]
[b]Gronli[39]
[c]Li et al.[41]
[d]McKinnon[40]
[e]Li[38]
[f]Lannon[32]

TABLE 6 Optimized set of MDF properties used in conjunction with the 1 Reaction Model

Virgin Material					
Parameter	Sample A	Sample B	Sample C	Sample D	Source
τ [m]	6.2×10^{-3}	4.1×10^{-3}	3.6×10^{-3}	3.2×10^{-3}	Measured
ρ [kg m^{-3}]	1090	890	890	1080	
k [W m^{-1} K^{-1}]	0.20	0.13	0.095	0.22	Fit to CC
c [J kg^{-1} K^{-1}]	2900	2900	2900	2650	
ε [−]	0.82	0.71	0.725	0.91	
α [m^2 kg^{-1}]	20	5	7	3	
h [J kg^{-1}]	-3.0×10^5	-4.0×10^5	-1.5×10^5	-1.2×10^6	
$\dot{m}''_{crit}$ [kg s^{-1} m^{-2}]	2.22×10^{-3}	2.33×10^{-3}	2.64×10^{-3}	2.13×10^{-3}	
θ_C [%]	17.5	14.4	17.6	11.6	Measured
A [s^{-1}]	1.44×10^7	5.81×10^7	4.80×10^6	2.80×10^8	Fit to MCC
E [J mol^{-1}]	1.04×10^5	1.15×10^5	1.019×10^5	1.223×10^5	
H_{eff} [J kg^{-1}]	11.3×10^6	11.7×10^6	10.3×10^6	12.9×10^6	Measured
Char					
ρ [kg m^{-3}]	191	128	382	255	Measured
k [W m^{-1} K^{-1}]	$9.5\times10^{-10}\times T^3$	$2.5\times10^{-10}\times T^3$	$1.25\times10^{-10}\times T^3$	$4\times10^{-10}\times T^3$	Fit to CC
α [m^2 kg^{-1}]	35	10	15	13	
c [J kg^{-1} K^{-1}]	1500	1500	1500	1500	Literature[38]
ε [−]	0.86	0.86	0.86	0.86	

exposure experiments were used to characterize the heat feedback from a square burner used as ignition source. Flame spread experiments were used to characterize the heat feedback from the flame growing on the corner walls.

During both burner exposure and flame spread experiments, the 30.5-cm-square and 35.4-cm-tall propane gas burner designed in accordance with NFPA 286[2] was positioned on the floor in the corner of the assembly. A mass flow controller was used to feed CP grade propane to the burner at a rate that would achieve the desired HRR based on a heat of combustion of propane equal to 46.4×10^6 J kg^{-1}.[43] Total flame heat flux to the wall was measured using an array of water-cooled Schmidt-Boelter heat flux gauges arranged vertically along one wall, flush with the wall surface. Heat flux gauges were separated from one another by 0.25 m (in the vertical direction) and placed 0.10 m from the corner to ensure that they were always located within the flame region. The gauges were cooled with water at a slightly elevated temperature of 313 K, to mitigate condensation on the gauge sensor surface.[44]

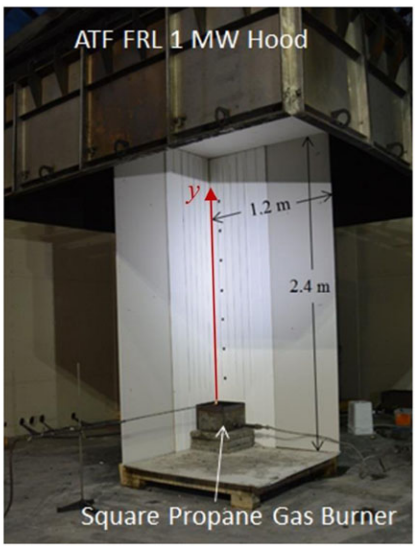

FIGURE 5 Open corner-wall setup [Colour figure can be viewed at wileyonlinelibrary.com]

The 1-MW exhaust hood was equipped with sampling and instrumentation to allow for oxygen consumption calorimetry that was used to obtain time resolved HRR measurements with an estimated uncertainty of 10% at 50 kW and 5% at 500 kW.[45] Two video cameras simultaneously recorded each test. One was positioned on the corner's bisection plane; the other faced one of the walls. The video collected by the latter (side-view) camera was used to estimate evolution of flame width along a single wall.

6.2 | Burner flame submodel

Burner flame heat flux, q''_b, was measured when the burner HRR was set to 40 kW. This HRR was used in both burner characterization experiments and in subsequent Room Corner Tests of the MDF materials. Burner characterization tests utilized noncombustible walls composed of gypsum wallboard. These walls were exposed to the burner for 200 s; tests were repeated 3 times. The average q''_b measurements are plotted in Figure 6A as points. These results indicate that the burner heat flux is transient. Over the first 30 s of the test, q''_b increases, in an approximately linear fashion, until it reaches a peak, steady-state value, $q''_{b,steady}$. This behavior is believed to be associated with a transient nature of the flame development over the surface of the burner. As seen in Figure 6B, $q''_{b,steady}$ varies with vertical distance above the top of the burner, y. Burner heat flux calculated using Lattimer's correlation[13] (the development of which is discussed in Section 2) is also shown in this figure.

Lattimer's burner flame heat flux correlation significantly overpredicts the heat fluxes measured in this work. Thus, a new correlation, which is shown as a solid line in Figure 6B, was developed to better capture these measurements:

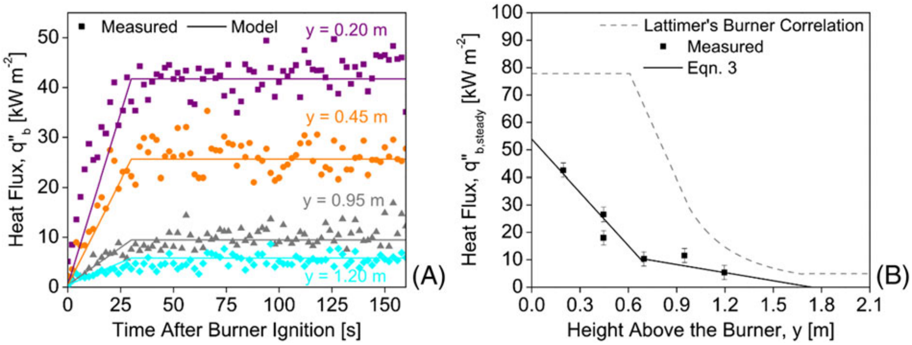

FIGURE 6 Measured and correlated burner flame heat fluxes to the corner walls (A) as a function of time and (B), in steady state, as a function of vertical position. The burner HRR was set at 40 kW [Colour figure can be viewed at wileyonlinelibrary.com]

$$q''_{b,steady}\left[\mathrm{kW\ m^{-2}}\right] = \begin{cases} -64.5\,y + 53.9, & 0<y\leq 0.7\,m \\ -9.9\,y + 17.2, & 0.7\,m<y\leq 1.7\,m \end{cases}. \quad (3)$$

This correlation was implemented as a time-dependent boundary condition in ThermaKin2D. It was assumed that the heat flux from the burner was radiative in nature.[46] The fact that $q''_{b,steady}$ is not reached instantaneously upon ignition of the burner was taken into account by scaling $q''_{b,steady}$ by a factor that varied linearly between 0 and 1 during the first 30 s of the exposure. The performance of this time-dependent model is demonstrated in Figure 6A (solid lines).

6.3 | Corner-wall flame submodel

To characterize heat feedback from the corner-wall flame, flame spread on Samples A, B, C, and D was initiated by exposing them to a 25-kW burner flame for 345, 227, 293, and 250 s, respectively. This burner HRR and the corresponding exposure times were selected based on an analysis of a preliminary series of experiments to minimize contribution of the igniter to the fire growth, while ensuring uniform ignition at the base of the sample. One test was performed on each MDF specimen; each specimen was stapled to the gypsum wallboard of the open corner-wall assembly. The HRR of the flame growing on the surface of these materials, the width of the luminous portion of the flame, and total flame heat flux to the corner walls (q''_f) were all measured as a function of time.

Figure 7 demonstrates the progression of the open corner-wall flame spread test for Sample B. Here, timestamps, t, indicate time after burner ignition. At t = 110 s, the sample ignited, and the fire size and flame height began to increase steadily until the propane burner was turned off at t = 227 s. After the burner was turned off, the fire decreased in size until it reached a minimum HRR of 28 kW. At t = 245 s, the HRR and flame height began to increase again, and flames spread vertically, reaching the ceiling at t = 347 s. At t = 530 s, the flames began to extend beyond the ceiling, at which point the fire was suppressed. Fire growth dynamics of Samples A and D were similar to that of Sample B: each material supported flame spread along the wall and the ceiling. Unlike these materials, Sample C self-extinguished shortly after the propane burner was turned off.

Except for Sample C, the width of the wall-material-supported flame varied little in time or from sample to sample. This width, taken along 1 wall of the corner, was determined to be 0.25 ± 0.05 m. Thus, the total width of the wall covered by the flame was 0.50 m. A complete set of the flame width data can be found in a related

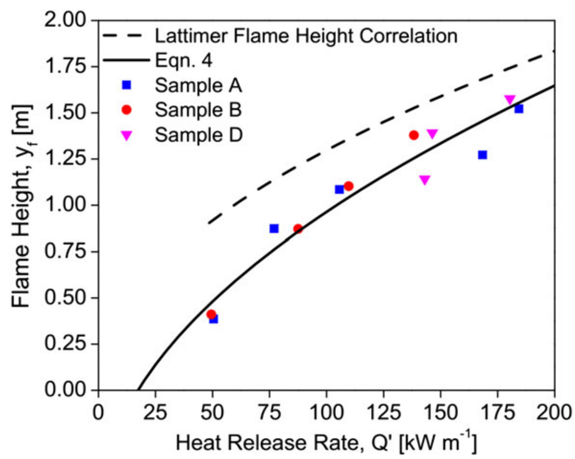

FIGURE 8 Flame height dependency on width-normalized heat release rate for the corner-wall flame [Colour figure can be viewed at wileyonlinelibrary.com]

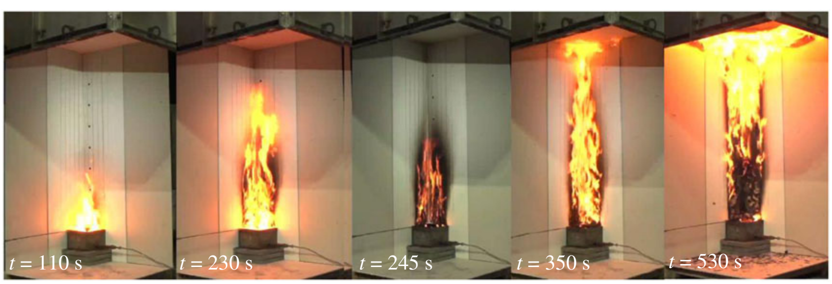

FIGURE 7 The open corner-wall flame spread on Sample B. t indicates time after burner ignition [Colour figure can be viewed at wileyonlinelibrary.com]

publication.[32] This parameter was used to compute width-normalized HRR (Q') by dividing the HRR measured after the burner was turned off by the total flame width (0.50 m).

Time resolved q''_f at all measurement locations (y, distance above top of the burner) tended to increase and reach a steady value of $q''_{f,steady}$= 42 ± 5 kW m^{-2} as the wall-material-supported flame spread, thickened, and became increasingly turbulent.[32] $q''_{f,steady}$ was found to be insensitive to variations in material composition and was therefore utilized to define flame height, y_f. Here, y_f is defined as the distance from the base of the flame to the highest location where measured heat flux is ≥85% of $q''_{f,steady}$. This definition of flame height explicitly accounts for movement of the base of the flame due to sample burnout. Figure 8 plots experimental measurements of y_f as a function of Q'. These flame height measurements can be correlated with width-normalized HRR measurements using an empirical expression of the form

$$y_f = a\left(Q'\right)^b + c \tag{4}$$

where a, b, and c are empirically derived constants. A similar definition of flame height was recently used to develop a flame heat feedback model for laminar wall flames.[47] Figure 8 demonstrates that by defining a, b, and c to be equal to 0.165, 0.50, and −0.69, respectively, the flame height derived from the experimental data can be fit with precision, R^2 = 0.93. The values of these constants correspond to y_f and Q' expressed in the units of m and kW m^{-1}, respectively. It should be noted that Sample C data were not included in this analysis because of its self-extinguishing behavior.

Also shown in Figure 8 (dashed line) are flame heights calculated using the corner-wall flame height correlation developed by Lattimer et al.[13] This correlation has a similar trend to that developed in this study; however, it calculates values of flame height that are systematically higher than those measured here. This discrepancy is likely a result of differences in measurement methodology: in Lattimer's study, flame height is defined based on image analysis as the maximum height of the continuous flame sheet rather than on the basis of heat flux measurements.

Based on the flame height correlation represented by Equation 4, a corner-wall flame heat feedback expression was parameterized. The functional form of this expression was based on that recently proposed for laminar wall flames[47,48]:

$$q''_f = \begin{cases} q''_{f,steady} & y_b \le y_f \\ \alpha_f\, q''_{f,steady}\, e^{-\ln(\alpha_f)\left(y^*\right)^2} & y_b > y_f \end{cases}. \tag{5}$$

$$y^* = \frac{y_b + y_0}{y_f + y_0} \tag{6}$$

where y_b is the height above the base of the flame. This expression assumes that the flame heat feedback profile consists of 2 distinct regions: the region below flame height ($y_b \le y_f$), where flame heat flux is constant and equal to $q''_{f,steady}$ (42 kW m^{-2}), and the region above the flame height (fire plume region) where flame heat flux decreases with height, due to air entrainment and radiative losses. The parameters describing this decrease, y_0 and α_f, were fit to best match q''_f measurements taken across the length of the sample, throughout the duration of experiments; y_0 = 2.0 m and α_f = 7.06 were found to represent the experimental data with a mean absolute error of 2.5 kW m^{-2}. The results of these fitting exercises are shown in Figure 9. This flame heat feedback model demonstrates high accuracy with respect to experimental measurements; however, care should be taken in its application to length scales or test configurations beyond those validated in this work.

This flame heat flux submodel was implemented in ThermaKin2D using an assumption that the heat flux is radiative in nature.[46] This model explicitly tracks the burnout height in both the flame height and flame heat feedback models. The Q' value required for Equation 4 was computed by integrating gaseous pyrolyzate mass flux, predicted by the pyrolysis submodel, over the height of the solid sample of unit width and by multiplying the integral by the corresponding heat of combustion. An additional implicit assumption used in both the burner and corner-wall flame submodels was that the heat feedback is spatially uniform along the width of the flame. This assumption is not fully justified, as the data provided in a related publication[32] indicate that the corner-wall flame heat flux decreases by almost 50% at the outer edge of the flame (0.25 m away from the corner). Nevertheless, this assumption was maintained here to avoid complications associated with the 3-dimensional treatment of this flame spread problem.

7 | ROOM CORNER EXPERIMENTS AND MODELING

7.1 | Room Corner Test setup and procedure

The Room Corner Test setup was performed in accordance with the NFPA 286 standard.[2] The test compartment, which was 2.4 × 3.6 m wide and 2.4 m tall, with a 0.8 × 2.0 m opening, is shown in Figure 10. Gypsum wallboard was installed along the walls and ceiling of the compartment. The MDF samples were stapled to all gypsum walls, except for the front wall where the door opening was located. The compartment assembly was positioned under the 4 MW rated exhaust hood located at the ATF FRL. This hood was equipped with oxygen consumption calorimetry that was used to obtain time resolved HRR measurements with an estimated uncertainty of 42%, 4.6%, and 2.6% at 50, 500, and 1100 kW, respectively.[49]

The same propane gas burner used in the open corner-wall experiments was also used in the Room Corner Tests. The burner HRR profile prescribed by the standard consists of 300 s of 40-kW exposure followed by 600 s of 160-kW exposure.[2] Preliminary tests indicated that this exposure was too severe for the MDF materials studied in this work as the fire growth was dominated by the burner itself rather than by the flame spread over the material surfaces. Therefore, a decision was made to reduce this exposure to 40 kW for 165 s, which emphasized flame-spread-driven fire growth.

Two critical times were determined based on visual observations of the fire: time to ceiling flame spread and time to flashover. Time

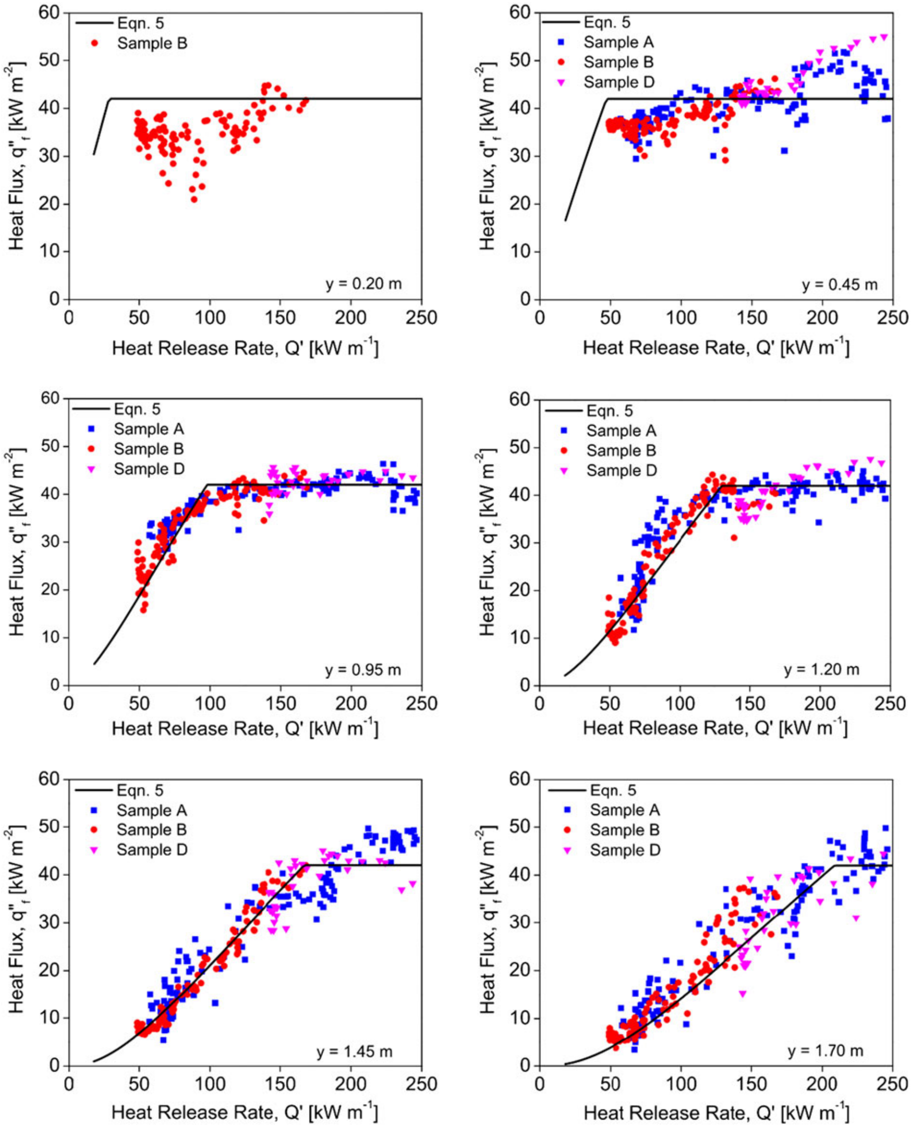

FIGURE 9 Corner-wall flame heat feedback at various heights, *y*, above the top of the burner as a function of width-normalized heat release rate [Colour figure can be viewed at wileyonlinelibrary.com]

FIGURE 10 Room Corner Test setup [Colour figure can be viewed at wileyonlinelibrary.com]

to ceiling flame spread is defined as the time when flames have spread upward along the entire corner wall and began to spread horizontally along the ceiling; this time was identified by a video camera located inside the compartment. This time is significant because, up to this point, fire growth is controlled by material behavior and not by secondary factors (such as radiation from ceiling smoke layer). Time to flashover is a key metric used to assess burning behavior in reconstructive fire tests; it is also a required test measurement in NFPA

TABLE 7 Summary of the Room Corner Test results

Sample	Test #	Time to Ceiling Flame Spread, s	Time to Flashover, s
A	1	532	717
	2	Self-extinguished	Self-extinguished
B	1	302	500
	2	282	440
C	1	Self-extinguished	Self-extinguished
D	1	234	345
	2	260	410

286 Room Corner Test reports.[2] Time to flashover can be defined by several metrics; in this work, it is defined as the moment when the flames extended beyond the door opening, in accordance with NFPA 286.[2] Two Room Corner Tests were performed for Samples A, B and D; only 1 test was performed for Sample C due to the limited availability of the laboratory facilities.

7.2 | Comparison of the test results with model predictions

Table 7 provides a summary of the Room Corner Test results. Although all of the tested materials were designated as MDF, they exhibited significant differences in fire behavior. Samples B and D supported relatively fast fire growth with the compartment reaching flashover within 500 s. The fire grew notably slower on Sample A: the fire reached flashover after 700 s in 1 test and self-extinguished in the other. Sample C also self-extinguished approximately 150 s after the burner was turned off. While only 1 test was conducted on Sample C, its self-extinguishing behavior was consistent with the results of the open corner-wall experiment, which indicates that Sample C was the least flammable among the tested MDF specimens.

The width-normalized heat release rate, Q', histories obtained in Room Corner Tests are shown in Figure 11 as points. The total flame width was assumed to be constant and equal to that measured in the open corner-wall experiments (0.50 m). The error bars correspond to the reported uncertainties of the HRR measurements. The Q' data do not include the contribution from the burner (it was subtracted). Measurements in Figure 11 are plotted up to Q' = 300–350 kW m^{-1} because this increase in Q' is dominated by the corner-wall flame spread and not by further fire growth across the ceiling of the compartment (Q' = 300–350 kW m^{-1} approximately corresponds to the times to ceiling flame spread given in Table 7). It is important to note that in every test where Q' reached 300 kW m^{-1}, Q' continued to increase, and flashover was observed within 100 to 200 s thereafter.

The model of these experiments realized in ThermaKin2D combined a pyrolysis submodel, which included a 2-dimensional (normal to the sample's surface and vertical) heat transport treatment and a 1-dimensional (normal to the sample's surface) mass transport treatment, with the burner and corner-wall flame submodels. As in the case of CC experiment modeling, the presence of the gypsum wallboard backing was simulated explicitly. In ThermaKin2D, the position of the base of the flame was determined by the lowest point on the sample surface where $\dot{m}''_{crit}$ (given in Table 6) was achieved. Flame ignition and extinction were defined using the flame height correlation expressed through Equation 4 (and plotted in Figure 8). The flame was considered to exist only when the computed flame height (y_f) achieved a positive value. To avoid "double counting" of the heat feedback to the material exposed to the burner flame, the heat feedback computed using the corner-wall flame model (Equation 5) was not applied until the burner was turned off. A brief study was conducted to ensure that the numerical integration parameters employed in these simulations provide fully converged results.[32]

The MDF materials were represented in the simulations by either the set of properties given in Table 6 (MCC and CC properties) or a set of properties combining virgin material densities and thicknesses (given in Table 1), MCC-derived heats of combustion (given in Table 2), MCC-derived kinetics (given in Table 3), and the average polymeric material properties provided in Table 5. The latter property

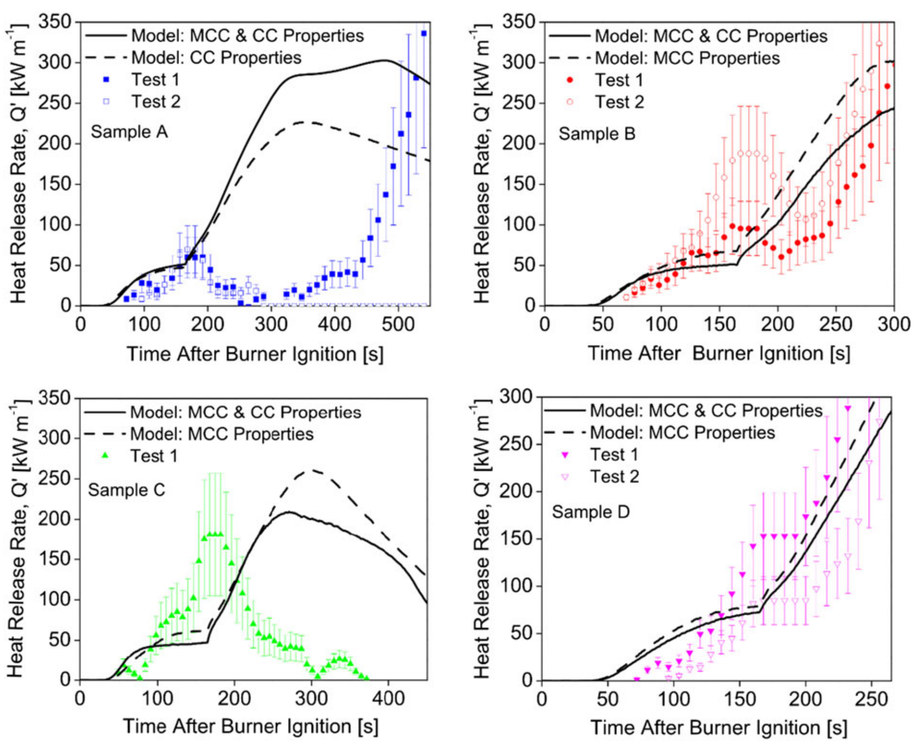

FIGURE 11 Experimentally measured and model predicted width-normalized heat release rate histories obtained for the Room Corner Tests of MDF materials. The contribution of the gas burner was subtracted from these data. The experimental uncertainties were computed from the stated uncertainties of the oxygen consumption calorimeter used in these tests [Colour figure can be viewed at wileyonlinelibrary.com]

set was constructed from the MCC-derived information and general knowledge about polymeric solids and, therefore, was designated as "MCC properties". Both property sets were based on the 1 Reaction Model kinetics.

The results of the simulations are shown as lines in Figure 11. The model based on the MCC and CC properties predicts the fire growth rate over Samples B and D well. This model also predicts Sample C fire growth dynamics reasonably well, ie, the model captures the value of the peak Q' and overall self-extinguishing behavior, although, the time of the peak is over-predicted. For Sample A, the model significantly under-predicts the onset time of fire growth but does correctly predict fire growth rate once flame spread occurs. The main reason for this discrepancy is probably associated with the fact that the Sample A's surface flame was extremely weak (consisting of flamelets distributed over the surface) during the 200 to 400-second time frame, and this weak flame was not adequately captured by the developed flame submodel. It should also be noted that the relative difference between model-predicted and experimentally measured CC HRRPUA was the greatest, on average, for Sample A (ie, uncertainties in the pyrolysis model parameters are also at least partially responsible for this discrepancy).

As expected, the MCC-properties-based model predictions were less accurate than those based on the MCC and CC properties; however, the differences between the modeled HRR curves were relatively small. This observation suggests that combining MCC data on a given material with typical thermo-physical property values provides a set of parameters that defines key features of material behavior in large-scale fires.

To further help differentiate full-scale performance of similar materials, an average fire growth rate (*FGR*) parameter was proposed. *FGR* is calculated from the given set of Q' data using the following expression:

$$FGR = \frac{Q'_{crit} - Q'_{b,off}}{t_{crit} - t_{b,off}}. \quad (7)$$

In this expression, $t_{b,off}$ is the time when the burner was turned off and $Q'_{b,off}$ is the corner-wall fire HRR at this time. Q'_{crit} is the critical HRR achievement which indicates that the fire will proceed to flashover; t_{crit} is the time at which Q'_{crit} is measured.

Based on the results of the current experiments, Q'_{crit} was set at 300 kW m^{-1}. If Q' = 300 kW m^{-1} was not reached during the test but Q' = 220 kW m^{-1} was reached, Q'_{crit} was assigned the maximum value of the HRR reached during the test. If Q' = 220 kW m^{-1} was never reached, the material was declared to exhibit self-extinguishing behavior and no *FGR* value was computed. The Q' = 220 kW m^{-1} threshold was selected because it approximately corresponded to the time when the corner-wall flame tips reached the compartment ceiling. It should be noted that *FGR* is similar to the fire growth rate parameter, FIGRA, defined in the ISO 9705 Room Corner[50] and Single Burning Item (EN 13823)[51] test standards; however, *FGR* is calculated based on critical values of Q' that emphasize fire growth when it is dominated by corner-wall flame spread (which is controlled by the wall lining material) and not by further fire growth across the ceiling of the compartment.

TABLE 8 Average fire growth rate (*FGR*) parameter computed for the experimental and model predicted results of the Room Corner Tests

		FGR [kW m^{-1} s^{-1}]		
Sample	Test #	Experimental	Modeled Using MCC and CC Properties	Modeled Using MCC Properties
A	1	0.7	0.9	1.0
	2	Self-extinguished		
B	1	1.5	1.3	1.8
	2	0.9		
C	1	Self-extinguished	Self-extinguished	1.5
D	1	2.2	2.1	2.5
	2	2.3		

FGR values were computed from the experimental and simulated data and are provided in Table 8. These values can be used to rate and compare the propensity of materials to spread flame. According to the experimental results, Sample D has the highest propensity followed by Sample B, Sample A, and Sample C. The model based on the MCC and CC properties provides similar *FGR* values, on average, they match within 20%, and identical relative ranking of the MDF specimens. For the model based on the MCC properties, model-predicted *FGR* are within 38% of experimental results, on average. Additionally, this model differs from experimental results somewhat in that it predicts that Sample C will spread the flame to the ceiling; however, the relative ranking of Samples A, B, and D in terms of fire growth rate remains the same. These results indicate that the proposed approach can be used to differentiate full-scale fire performance of similar materials, especially when the pyrolysis model parameters are derived from a combination of milligram-scale and bench-scale testing. The modeled scenario can be easily adjusted in its severity to match the fire being reconstructed by changing either the burner heat feedback and/or timing of the simulated exposure.

8 | CONCLUSIONS

A new procedure has been developed for fire investigators that can be used to determine how much similar materials contribute to fire growth in a full-scale reconstruction fire test. This procedure defines a quantitative methodology to assess the suitability of a candidate material for use in reconstructive fire tests. This procedure requires fire investigators to obtain the properties of both the material collected at the scene and of candidate samples through inverse analysis (numerical modeling) of either MCC-only or MCC and CC experiments; each approach can be used to differentiate the full-scale fire performance of similar materials. The properties of candidate materials can be stored in a database, which, in time, should minimize or completely eliminate the need for candidate material testing and analysis.

The MCC-only approach is significantly less labor intensive and requires only a small (approximately 50 mg) material sample (it is assumed that the sample is sufficiently representative to correctly determine the overall density and thickness of the virgin material). The time, effort, and sample amount required for the MCC and CC approach are each significantly greater; however, this approach does produce more accurate results. It should be noted that, for each of these approaches, the required sample amount is still many times smaller than that usually needed for a full-scale reconstructive fire experiment.

Once its properties are determined, the relative performance of a candidate material is evaluated by simulating the early stages of the Room Corner Test using the ThermaKin2D numerical modeling framework. These simulations require submodels for heat feedback from the burner (ignition source) and from the corner-wall flame supported by the burning material, both of which were developed in this study. It is expected that, even though the corner-wall flame heat feedback submodel was developed using only MDF materials, it is applicable to a wide range of polymeric solids.

The unified model of material pyrolysis and flame heat feedback has been shown to produce sufficiently accurate predictions of early fire growth to correctly discriminate fire spread performance of different brands of MDF. An average fire growth rate parameter (*FGR*) was proposed to formally rate each material in terms of its propensity to support full-scale fire growth. Application to a wider range of materials will be required to fully establish this methodology's capabilities and limitations.

ACKNOWLEDGEMENTS

The authors would like to thank Jason Dress, Brian Grove, Cory Runyon, John Butta, Mark Gratkowski, Rob Wulff, Steve Little, James Zurenko and Adam St. John of the ATF Fire Research Laboratory and Xi Ding, Dr Fernando Raffan, Dr Mark McKinnon, Dr James Milke and Dr Arnaud Trouvé of the University of Maryland. This project would not be possible without help and support from these individuals.

ORCID

Stanislav I. Stoliarov http://orcid.org/0000-0002-3429-9245

REFERENCES

1. NFPA 921. *Guide for Fire and Explosion Investigations*. Quincy, MA: National Fire Protection Association; 2013.
2. NFPA 286. *Standard Methods of Fire Tests for Evaluating Contribution of Wall and Ceiling Interior Finish to Room Fire Growth*. Quincy, MA: National Fire Protection Association; 2006.
3. Karlsson B, Quintiere JG. *Enclosure Fire Dynamics*. Boca Raton, Fl: CRC Press; 2000:657-666.
4. Saito K, Quintiere JG, Williams F. Upward turbulent flame spread. *Fire Safety Sci*. 1986;1:75-86.
5. Williamson R, Revenaugh A, Mowrer F. Ignition sources in room fire tests and some implications for flame spread evaluation. *Fire Safety Sci*. 1991;3:657-666.
6. Kokkala MA. *Characteristics of a Flame in an Open Corner of Walls, Interflam '93*. London: Interscience Communications:13-29.
7. Tran HC, Janssens ML. Modeling the burner source used in the ASTM room fire test. *J Fire Prot Eng*. 1993;5(2):53-66.
8. Quintiere JG, Cleary TG. Heat flux from flames to vertical surfaces. *Fire Technol*. 1994;30(2):209-231.
9. Hasemi Y, Yoshida M, Takashima S, Kikuchi R, Yokobayashi Y. *Flame Length and Flame Heat Transfer Correlations in Corner-Wall and Corner-wall-ceiling Configurations, Interflam '96*. London: Interscience Communications:179-188.
10. Qian C, Saito K. An empirical model for upward flame spread over vertical flat and corner walls. *Fire Safety Sci*. 1997;5:285-296.
11. Ohlemiller T, Cleary T, Shields J. Effects of ignition conditions on upward flame spread on a composite material in a corner configuration. *Fire Saf J*. 1998;31(4):331-344.
12. Dillon S. *Analysis of the ISO 9705 Room/Corner Test: Simulations, Correlations and Heat Flux Measurements, NIST-GCR-98-756 Report*. Gaithersburg, MD: National Institute of Standards and Technology; 1998.
13. Lattimer BY, Sorathia U. Thermal characteristics of fires in a noncombustible corner. *Fire Saf J*. 2003;38(8):709-745.
14. Lattimer BY, Sorathia U. Thermal characteristics of fires in a combustible corner. *Fire Saf J*. 2003;38(8):747-770.
15. Quintiere JG. A simulation model for fire growth on materials subject to a room corner test. *Fire Saf J*. 1993;20(4):313-339.
16. Wade C. *A New Engineering Tool for Evaluating the Fire Hazard in Rooms, BRANZ Study*. Report 66, Building Research Association of New Zealand, Judgeford, Porirua City, New Zealand (1999).
17. Van Hees P, Hertzberg T, Hansen AS. *Development of a Screening Method for the SBI and Room Corner using the Cone Calorimeter*. Sweden: SP Swedish National Testing and Research Institute; 2002.
18. Lattimer BY, Hunt SP, Wright M, Beyler C. Corner fire growth in a room with a combustible lining. *Fire Safety Sci*. 2003;7:419-430.
19. Janssens M, Huczek J, Gomez C. Modeling of the performance of GRP panels in the ISO 9705 room test. *Compos Polycon*. 2009.
20. Grexa O, Dietenberger MA, White RH. *Reaction-to-Fire of Wood Products and Other Building Materials, FPL-RP-663*. Forest Products Laboratory, Madison, WA: United States Department of Agriculture; 2012.
21. ASTM Standard E1354-13. *Standard Test Method for Heat and Visible Smoke Release Rates for Materials and Products Using an Oxygen Consumption Calorimeter*. West Conshohocken, PA: ASTM International; 2014.
22. ASTM Standard E1321–13. *Standard Test Method for Determining Material Ignition and Flame Spread Properties*. West Conshohocken, PA: ASTM International; 2013.
23. Wade CA. BRANZFIRE technical reference guide, BRANZ Study Report 92 (revised), Building Research Association of New Zealand, Judgeford, Porirua City, New Zealand, 2008.
24. Stoliarov SI, Leventon IT, Lyon RE. Two-dimensional model of burning for pyrolyzable solids. *Fire Mater*. 2014;38(3):391-408.
25. Stoliarov SI, Li J. Parameterization and validation of pyrolysis models for polymeric materials. *Fire Technol*. 2016;52(1):79-91.
26. ASTM Standard D7309. *Standard Test Method for Determining Flammability Characteristics of Plastics and Other Solid Materials Using Microscale Combustion*. West Conshohocken, PA: ASTM International; 2013.
27. Stoliarov SI, Safronava N, Lyon RE. The effect of variation in polymer properties on the rate of burning. *Fire Mater*. 2009;33(6):257-271.
28. Chaos M, Khan MM, Krishnamoorthy N, de Ris JL, Dorofeev SB. Evaluation of optimization schemes and determination of solid fuel properties for CFD fire models using bench-scale pyrolysis tests. *Proc Combust Inst*. 2011;33(2):2599-2606.
29. Li J, Stoliarov SI. Measurement of kinetics and thermodynamics of the thermal degradation for charring polymers. *Polym Degrad Stab*. 2014;106:2-15.
30. McKinnon MB, Stoliarov SI. Pyrolysis model development for a multilayer floor covering. *Materials*. 2015;8(9):6117-6153.
31. Li K, Huang X, Fleischmann C, Rein G, Ji J. Pyrolysis of medium density fibreboard: optimized search for kinetic scheme and parameters via genetic algorithm driven by Kissinger's method. *Energy Fuel*. 2014;28(9):6130-6139.
32. Lannon CA. Methodology for determining the fire performance equivalency amongst similar materials during a full-scale fire scenario based

on bench-scale testing, Department of Fire Protection Engineering, University of Maryland, Masters Thesis, 2015.
33. Beaulieu PA, Dembsey NA. Effect of oxygen on flame heat flux in horizontal and vertical orientations. *Fire Saf J*. 2008;43(6):410-428.
34. Stoliarov SI, Crowley S, Lyon RE, Linteris GT. Prediction of the burning rates of non-charring polymers. *Combust Flame*. 2009;156(5):1068-1083.
35. Stoliarov SI, Crowley S, Walters RN, Lyon RE. Prediction of the burning rates of charring polymers. *Combust Flame*. 2010;157(11):2024-2034.
36. Rahmanian I. Thermal and mechanical properties of gypsum boards and their influences on fire resistance of gypsum board based systems, University of Manchester, PhD Dissertation; 2011.
37. Li J, Stoliarov SI. Development of pyrolysis models for charring polymers. *Polym Degrad Stab*. 2015;115:138-152.
38. Li J. A multiscale approach to parameterization of burning models for polymeric materials, University of Maryland, PhD Dissertation, 2014.
39. Gronli MG. A theoretical and experimental study of the thermal degradation of biomass, The Norwegian University of Science and Technology, Doctoral Thesis, Trondheim, Norway, 1996.
40. McKinnon MB. Development of a model for flaming combustion of double-wall corrugated cardboard, Department of Fire Protection Engineering, University of Maryland, Masters Thesis, 2012.
41. Li KY, Fleischmann CM, Spearpoint MJ. Determining thermal physical properties of pyrolyzing New Zealand medium density fibreboard (MDF). *Chem Eng Sci*. 2013;95:211-220.
42. Lyon RE, Quintiere JQ. Criteria for piloted ignition of combustible solids. *Combust Flame*. 2007;151(4):551-559.
43. DiNenno PJ. *SFPE Handbook of Fire Protection Engineering*. 4th ed. MA, Table C.2: National Fire Protection Association Quincy; 2008.
44. Bureau of Alcohol, Tobacco, Firearms and Explosives Fire Research Laboratory, Laboratory Instruction: Heat Flux Transducers, LI002, Ammendale, MD.
45. Bureau of Alcohol, Tobacco, Firearms and Explosives Fire Research Laboratory, Technical Reference: Fire Products Collector—1 MW Square, TR011a, Ammendale, MD.
46. Fernandez-Pello AC, Hirano T. Controlling mechanisms of flame spread. *Combust Sci Technol*. 1983;32(1-4):1-31.
47. Leventon IT, Korver KT, Stoliarov SI. A generalized model of flame to surface heat feedback for laminar wall flames. *Combust Flame*. 2017;179:338-353.
48. Leventon IT, Li J, Stoliarov SI. A flame spread simulation based on a comprehensive solid pyrolysis model coupled with a detailed empirical flame structure representation. *Combust Flame*. 2015; 162(10):3884-3895.
49. Bureau of Alcohol, Tobacco, Firearms and Explosives Fire Research Laboratory, Technical reference: fire products collector—4 MW TR011c, Ammendale, MD.
50. ISO 9705–1. *Reaction to Fire Tests—Room Corner Test for Wall and Ceiling Lining Products; Part* 1: Test Method for a Small Room Configuration, International Organization for Standardization, Geneva, Switzerland, 2016.
51. EN 13823:2010+A1:2014. *Reaction to Fire Tests for Building Products—Building Products Excluding Floorings Exposed to the Thermal Attack by a Single Burning Item*. Brussels, Belgium: European Committee for Standardization; 2014.

SUPPORTING INFORMATION

Additional Supporting Information may be found online in the supporting information tab for this article.

How to cite this article: Lannon CM, Stoliarov SI, Lord JM, Leventon IT. A methodology for predicting and comparing the full-scale fire performance of similar materials based on small-scale testing. *Fire and Materials*. 2018;42:710–724. https://doi.org/10.1002/fam.2524